Antiviral Research 161 (2019) 125–133

Contents lists available at ScienceDirect

Antiviral Research

journal homepage: www.elsevier.com/locate/antiviral

Establishment of a lethal aged mouse model of human respiratory syncytial virus infection

Ke Zhang[a,b,c], Cun Li[a], Yu-Si Luo[a], Lei Wen[a], Shuofeng Yuan[a], Dong Wang[a], Bosco Ho-Yin Wong[a], Xiaoyu Zhao[a], Man Chun Chiu[a], Zi-Wei Ye[a], Zehua Sun[a], Hanjun Zhao[a], Xiaomin Zhang[a], Meng Hu[a], Dong Yang[a], Huiping Shuai[a], Yixin Wang[a], Jie He[d], Michael E. Bose[d], Kelly J. Henrickson[d], Jian-Dong Huang[e], Bojian Zheng[a], Hin Chu[a,f,g,**], Jie Zhou[a,f,g,*]

[a] Department of Microbiology, The University of Hong Kong, Hong Kong, China
[b] Department of Parasitology, Basic Medical College, Guizhou Medical University, Guiyang, China
[c] The Key and Characteristic Laboratory of Modern Pathogen Biology, Guizhou Medical University, Guiyang, China
[d] Department of Pediatrics, Medical College of Wisconsin, Milwaukee, WI, USA
[e] School of Biomedical Sciences, The University of Hong Kong, Hong Kong, China
[f] State Key Laboratory of Emerging Infectious Diseases, The University of Hong Kong, Hong Kong, China
[g] Research Centre of Infection and Immunology, The University of Hong Kong, Hong Kong, China

ARTICLE INFO

Keywords:
Human respiratory syncytial virus
Lethal mouse model
Lung pathology
Genome mutation

ABSTRACT

Human respiratory syncytial virus (HRSV) infection is a significant cause of morbidity and mortality, particularly among the children and the elderly. Despite extensive efforts, there is currently no formally approved vaccine and effective antiviral options against HRSV infection are limited. The development of vaccines and antiviral strategies for HRSV was partly hampered by the lack of an efficient lethal mouse model to evaluate the efficacy of the candidate vaccines or antivirals. In this study, we established a lethal HRSV mouse model by consecutively passaging a clinical HRSV isolate, GZ08-0. GZ08-18 was isolated from mouse bronchioalveolar lavage fluids at the 50th passage of GZ08-0. Importantly, all GZ08-18-inoculated mice succumbed to the infection by day 7 post infection, whereas all GZ08-0-inoculated mice recovered from the infection. Subsequent investigations demonstrated that GZ08-18 replicated to a higher titer in mouse lungs, induced more prominent lung pathology, and resulted in higher expression levels of a number of key pro-inflammatory cytokines including IFN-γ, MIP-1α, and TNF-α in comparison to that of GZ08-0. The cyclophosphamide pretreatment rendered the mice more susceptible to a lethal outcome with less rounds of virus inoculation. Full genome sequencing revealed 17 mutations in GZ08-18, some of which might account for the dramatically increased pathogenicity over GZ08-0. In addition, by using ribavirin as a positive control, we demonstrated the potential application of this lethal mouse model as a tool in HRSV investigations. Overall, we have successfully established a practical lethal mouse model for HRSV with a mouse-adapted virus, which may facilitate future in vivo studies on the evaluation of candidate vaccines and drugs against HRSV.

1. Introduction

Human respiratory syncytial virus (HRSV) is the most common cause of acute lower respiratory tract infection (ALRTI) and the major cause of hospitalization from severe ALRTI in children under 5 years old (Falsey et al., 2005; Thompson et al., 2003). It was estimated that more than 33 million children younger than 5 years old were infected by HRSV, leading to over 3 million hospitalizations and approximately 200,000 deaths in 2005 (Nair et al., 2010). HRSV infection is also a significant cause of morbidity and mortality in the elderly, immunocompromised individuals, and patients with chronic underlying illnesses. Data from public health investigations suggested that the challenge of HRSV infection among the elderly was more urgent than that of pandemic influenza (Falsey et al., 2005; Shaw et al., 2013). Unfortunately, despite active research in the past decades, there has been limited effective antiviral treatment and no formally-approved

* Corresponding author. Department of Microbiology, the University of Hong Kong, Queen Mary Hospital, 102 Pokfulam Road, Pokfulam, Hong Kong, China.
** Corresponding author. Department of Microbiology, The University of Hong Kong, Hong Kong, China.
E-mail addresses: hinchu@hku.hk (H. Chu), jiezhou@hku.hk (J. Zhou).

https://doi.org/10.1016/j.antiviral.2018.11.015
Received 26 April 2018; Received in revised form 27 November 2018; Accepted 29 November 2018
Available online 29 November 2018
0166-3542/

vaccine for HRSV infection.

Modeling HRSV disease in experimental animals is an essential step in the search for novel therapeutic agents and preventive measures, as well as for understanding the pathogenesis of HRSV infection. Non-human primate, including chimpanzee and African green monkey, and other animals such as lamb, sheep, and bovine have been used for HRSV research (Jordan et al., 2015; Sow et al., 2011; Tang et al., 2004; Teng et al., 2000). Nevertheless, those animals are neither available nor readily practicable for most laboratories due to various known restrictions. Currently, BALB/c mouse is the most commonly used HRSV animal model due to the clear genetic background, availability of abundant biological reagents, and cost effectiveness. Although HRSV can infect BALB/c mouse and cause illnesses and lung pathology, the infection is not fatal. In this regard, the BALB/c mouse model is defined as a semi-permissive model for HRSV infection (Graham, 2011; Graham et al., 1988). In 2005, Bolger et al. demonstrated that HRSV could result in lethal infection in young BALB/c mouse when challenged at a high inoculum (Bolger et al., 2005). However, a considerable amount of effort is required to generate the virus stock at high enough titer, which may render the application of this model challenging for a number of laboratories.

In this study, we seek to establish a more practical lethal mouse model through generating mouse-adapted viruses by passaging the virus in mice. To this end, we utilized a clinically isolated HRSV A strain (GZ08-0, GenBank accession No, KP218910) as the parental virus to inoculate aged BALB/c mice since RSV grew to higher titer in aged mice than in young mice (Taylor et al., 1984). After 50 successive passages in aged BALB/c mice, four strains of virus were isolated. One of the isolates, GZ08-18 (GenBank accession No, KP119747) (Zhang et al., 2015) resulted in increased virulence and fatality in aged BALB/c mice. Downstream investigations revealed that GZ08-18 replicated to a higher level in the mice lungs than that of GZ08-0. At the same time, GZ08-18 infection resulted in an exaggerated expression of pro-inflammatory cytokine and a more prominent lung pathology, which might explain its elevated virulence. Importantly, to demonstrate the capacity of the lethal mouse model as a platform for HRSV studies, we showed that ribavirin treatment completely prevented mice death after GZ08-18 challenge while the control-treated mice all succumbed to the virus by day 7 post infection. Altogether, our study established the first practical lethal HRSV mouse model with mouse-adapted virus that would contribute to the investigations on anti-HRSV treatments as well as studies on the pathogenesis of severe HRSV infections.

2. Materials and methods

2.1. Cells

HEp-2 cells were cultured with the standard protocol of American Type Culture Collection with some modifications. Briefly, HEp-2 cells were grown in T75 tissue culture flasks using DMEM/F12 GlutaMax-I (10,565, Gbico Ltd, USA) supplemented with 5% fetal bovine serum (FBS) and 1% penicillin/streptomycin (P/S) in a 37 °C incubator with 5% CO_2. The cells were passage every 3 days at a confluence of approximately 80%.

2.2. Viruses and plaque purification

GZ08-0 was clinically isolated as previously described (Zhang et al., 2015). GZ08-18 was isolated with plaque purification from the 50th passage of GZ08-0 in aged BALB/c mice. Plaque purification of GZ08-18 and other isolates were performed as described previously (McKimm-Breschkin, 2004). In brief, HEp-2 cells were seeded into a 12-well plate. When cell confluence reached 90%, the supernatant was removed and cells were washed once with PBS. Viruses were added into duplicated wells with 10-fold diluted MOI (500 µl/well). The virus was allowed to infect the cells for 4 h in a 37 °C incubator with 5% CO_2 with manual shaking every 20 min. In the meantime, the overlay consisting of 0.6% ICN immunodiffusion grade agarose (0895,201, MP Biomedicals, LLC) dissolved in PBS was autoclaved and then kept in a 55 °C water bath. The HEp-2 cell culture medium was also warmed in a 37 °C water bath. After 4 h, the virus inoculum was removed and cells were washed once with PBS. Equal volume of 0.6% immunodiffusion agar and HEp-2 cell culture medium was mixed as the overlay medium and was added into the wells at 3 ml/well. After gel solidification, the plate was incubated in a 37 °C incubator with 5% CO_2. Generally, plaques were visible by eyes at day 4 to day 5 post infection. Each visible plaque would be selected carefully with sterilized cloning cylinders and separately cultured in HEp-2 cells, which were subsequently subjected to whole genome sequencing.

2.3. Serial passage of HRSV in aged BALB/c mice

All mouse experiments were approved by Committee of the Use of Live Animals in Teaching and Research, the University of Hong Kong. BALB/c female retired breeders of 8–10 months old with body weight of 32.72 ± 2.59 g (mean ± SD) were used for the study. The virus was administrated to 3 aged BALB/c mice via intra-tracheal inoculation as described previously (Dupage et al., 2009). At day 3 post infection, BALF was harvested according to a protocol adopted from a previous publication (Daubeuf and Frossard, 2012). The virus titers of BALF for passages 20, 30, 40, and 50 were measured with the 50% tissue culture infective dose ($TCID_{50}$) assay. To inoculate the next round of mice for the serial passage, the BALF was inoculated in HEp-2 cells. After 72 h, the supernatant was harvested. A 100 µl aliquot of the supernatant was used to inoculate the next round of mice, meanwhile the supernatant was titrated with the $TCID_{50}$ assay (Supplementary Fig. S1). In this study, a total of 50 consecutive passages were performed. GZ08-18 was plaque purified from the BALF of infected mice from the 50th passage.

2.4. Virus propagation for mouse experiments

GZ08-0 or GZ08-18 were propagated in HEp-2 cells in a T75 flask. HEp-2 cells were seeded in a T75 flask with DMEM/F12 GlutaMax-I medium plus 5% FBS and 1% P/S at 37 °C with 5% CO_2. On the day after, the cells were infected with 3 ml DMEM/F12 GlutaMax-I medium containing GZ08-0 or GZ08-18 at a MOI of 0.4 for 1 h in an incubator at 37 °C and 5% CO_2. After inoculation, the cells were washed once with phosphate buffered saline (PBS). DMEM/F12 GlutaMax-I medium of 10 ml supplemented with 2% FBS and 1% P/S were added into the flask and incubated for 72 h. Afterwards, the culture supernatant was removed and replaced with 3 ml of DMEM/F12 GlutaMax-I supplemented with 40% glycerol and 10% FBS (pH 7.5). The cells were subjected to 3 freeze-thaw cycles (−70 °C/1min followed by 4 °C/1min). Subsequently, the cell suspension was centrifugated 4,000 g for 20 min at 4 °C to remove cell debris. The supernatant was aliquoted and stored in −80 °C for mouse experiments.

2.5. Intra-tracheal virus inoculation

GZ08-0 or GZ08-18 at 10^{10} $TCID_{50}$ per 100 µl was administrated to aged BALB/c mice via intra-tracheal inoculation as described previously (Dupage et al., 2009) with some modification. Briefly, after anesthesia, the mouse was put on a soft pad with its upper teeth hooked on a steel wire. A fiber optic light source (Euromex Iluminator EK-1, Holland) was applied to provide cool lighting against the mouse throat. Before the inoculation, sterilized blunt forceps, 24G Surflo® I.V. Catheter (Terumo Corp, Philippines), and P100 pipetman were prepared. The needle of the catheter was set in a backward position to avoid injury to the mouse trachea. Forceps were used to pull the tongue out to expose the inlet of the trachea, meanwhile the catheter was inserted into the trachea. The needle of the catheter was then drawn out and 100 µl of virus inoculum was injected to the catheter with a P100

pipetman.

2.6. Bronchoalveolar lavage fluid (BALF) collection

Harvesting BALF was performed according to a protocol adopted from a previous publication (Daubeuf and Frossard, 2012). In brief, after the mouse was sacrificed, the trachea and lung were carefully removed and perfused with 800 µl of DMEM/F12 GlutaMAX-I medium using a 22G Surflo I.V. catheter (Terumo Corp, Philippines). The medium was supplemented with antibiotics cocktail including Vancomysin (20 µg/ml), Ciprofloxacin (20 µg/ml), Amikacin (0.05 µg/ml), Nystatin (50 µg/ml), Penicillin (100 unit/ml), and Streptomycin (100 µg/ml). The resultant BALF, with an approximate volume of 400–600 µl per mouse, was then centrifuged at 10,000 rpm for 5 min. The supernatant was used to infect HEp-2 cells for virus propagation or $TCID_{50}$ assay and RT-qPCR assay for virus titration.

2.7. HRSV infection of BALB/c mice and sample collection

After anesthesia, the mice were intra-tracheally inoculated with 10^{10} $TCID_{50}$ of the viruses, for totally five times at a 12-h interval. At the indicated time points after the last virus inoculation, 3 mice in each group were sacrificed for the detection of viral growth. BALF samples of the mice were collected for viral load quantification by $TCID_{50}$ assay and RT-qPCR assay, as well as the detection of albumin by ELISA assay. For a subset of experiments, 3 mice in each group were sacrificed on the indicated day post infection. The right lobes of the mouse lung were homogenized for the detection of proinflammatory cytokines/chemokines by ELISA and the left lobes were fixed with 4% paraformaldehyde for histopathology examination and immunostaining of viral antigen. Mouse survival rate and body weight were monitored up to day 21 post infection.

2.8. Cyclophosphamide (CYP) pretreatment

We assessed whether the pretreatment of CYP can increase HRSV pathogenicity as reported previously (Kong et al., 2005). Briefly, a single dose of CYP (150 mg/kg body weight, Sigma, St. Louis, MO) was intraperitoneally administered to mice. On day 6 after CYP treatment, the mice were intra-tracheally inoculated with GZ08-0 or GZ08-18 (10^{10} $TCID_{50}$ in 100 µl) for two times at a 12 h-interval. Mouse survival and body weight change were monitored up to day 21 post infection.

2.9. Ribavirin treatment of the lethal model

To evaluate the anti-HRSV effect of ribavirin on our lethal HRSV mouse model, 0.9% NaCl-dissolved ribavirin (100 mg/kg body weight, Solarbio Ltd, China) was intraperitoneally administered to 10 mice at 3 h post infection after the 2nd, 4th, and 5th GZ08-18 inoculation. PBS was intraperitoneally administered to 8 GZ08-18 inoculated mice at the same time points as the control group. Mouse survival and body weight change were recorded daily and monitored up to day 21 post infection. In another set of experiment, we compared the viral titers in the BALF samples from 18 ribavirin-treated mice and 18 PBS-treated mice after the same inoculation procedure. Six mice in each group were sacrificed on day 2, day 3, and day 4 post infection. The BALF samples were collected and titrated by $TCID_{50}$ assay.

2.10. Detection of viral replication

The viral growth in the infected mice was measured with 50% tissue culture infective dose ($TCID_{50}$) assay and RT-qPCR assay. For virus titration, aliquots of BALF samples, brain homogenates and mouse blood were applied to $TCID_{50}$ assay on confluent HEp-2 cells in 96-well plates. Briefly, serial 10-fold dilution of each sample was inoculated in HEp-2 cell monolayer in sextuplet and cultured in penicillin/streptomycin-supplemented DMEM/F12 GlutaMAX-I. The cells were observed for CPE for 4–5 days. Viral titer was calculated with Spearman-Karber method. One $TCID_{50}$ is interpreted as the amount of virus that causes CPE in 50% of inoculated wells. For RT-qPCR assay, mouse samples were used for RNA extraction with QIAamp Viral RNA Mini Kit (Qiagen), followed by reverse transcription using Prime Script II 1st Strand cDNA Synthesis Kit (Clontech). The resultant cDNAs were applied to RT-qPCR assay using forward primer (5′-CTCAATTTCCTCACT TCTC-3′) and reverse primer (5′-CCTCTGTATTCTCCCATT-3′) as described previously (Do et al., 2012). The plasmid with partial HRSV N gene was constructed and used as the standards for absolute quantification.

2.11. Histopathological examination and immunofluorescence staining of mouse lung tissue

Mice were sacrificed and the lungs were removed and immediately fixed in 4% paraformaldehyde (PFA). The fixed lung tissues were processed and sectioned into paraffin sections of 6 µm in thickness. Hematoxylin and eosin (H&E) staining was performed on paraffin sections using standard method. The slides of mouse lung at day 3 post infection were used for immunofluorescence staining. Antigen retrieval, permeabilization, and blocking procedures were performed as previously described (Chu et al., 2018). Subsequently, the slides were labeled with mouse monoclonal antibody against HRSV fusion (F) protein (Santa Cruz, sc-101362), followed by Alexa Fluor 488 goat anti-mouse IgG (Life Technologies, R37120) as described previously (Sun et al., 2017; Zhou et al., 2014; Chu et al., 2016). Tissue slides were mounted with ProLong Diamond Antifade Mountant with DAPI (Life Technologies) and imaged using Carl Zeiss LSM 800 confocal microscope.

2.12. Detection of cytokines/chemokines and albumin by ELISA

The lung homogenates harvested from GZ08-0 and GZ08-18 inoculated mice were used for the detection of IFN-γ, MIP-1α, TNF-α, RANTES, and IFN-β using ProcartaPlex Multiplex Immunoassay (Thermo Fisher Scientific); while the BALF samples of GZ08-0 and GZ08-18 inoculated mice were harvested for the detection of albumin with ELISA (Bethyl Laboratories Inc, USA, E99-134).

2.13. Quantification of lung pathology

To quantify the lung pathology of GZ08-0- and GZ08-18-infected mice, the HE slides were examined in a blinded manner and scored with a semi-quantitative system according to the relative degree of inflammation and tissue damage as we previously described (Ye et al., 2017). Inflammation was scored as follows: 0, no inflammation; 1, perivascular cuff of inflammatory cells; 2, mild inflammation (extending throughout 25% of the lung); 3, moderate inflammation (25–50% of the lung); 4, severe inflammation involving over one half of the lung.

2.14. Sequencing and bioinformatics analysis of GZ08-0 and GZ08-18

Sequencing of GZ08-0 and GZ08-18 was described previously (Zhang et al., 2015). The amino acid sequences of GZ08-0 and GZ08-18 were analyzed in ExPASy (http://prosite.expasy.org/prosite.html) to interpret the possible functional alternations of non-synonymous mutations.

2.15. Statistical analysis

The increased viral titers after consecutive passaging as shown in Fig. 1 were analyzed using one-way ANOVA for variance and Bonferroni post-hoc tests. The two-tailed Student's *t*-test was used to analyze the body weight change of two groups of mice. Mann-Whitney test was

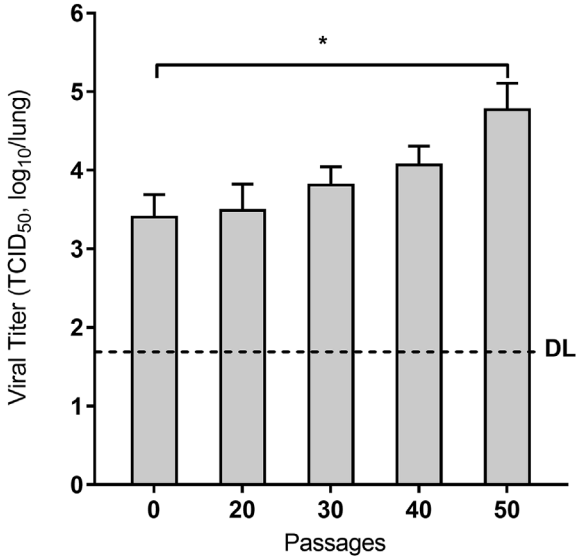

Fig. 1. HRSV showed increased viral titers after consecutive passage in aged BALB/c mice. GZ08-0 was passaged in aged BALB/c mice as described in Methods. The BALF samples collected from the mice at the 20th, 30th, 40th, and 50th passages and those from GZ08-0 inoculated mice were titrated with $TCID_{50}$ assay. Data represent mean +SD of 3 mice. DL, Detect Limitation. * represents $p < 0.05$.

applied to compare the viral loads and ELISA results. Mouse survival was analyzed with Log rank test. A *P* value less than 0.05 was considered to be statistically significant.

3. Results

3.1. The adaptation of HRSV through serial virus passages in aged BALB/c mice

In order to obtain a mouse-adapted HRSV strain, we successively passaged GZ08-0 in aged BALB/c mice. We examined the viral titers in BALF samples from the infected mice at the 20th, 30th, 40th, and 50th passages, together with those from the GZ08-0 inoculated mice. We noticed that viruses isolated from the later passages replicated to higher titers than that of the viruses isolated from earlier passages as the virus was consecutively passaged in mice. Importantly, the viral titer in BALF samples collected from the 50th passage was significantly higher than that from the GZ08-0 inoculated mice (Fig. 1). Thus, the result suggested that HRSV gradually adapted and replicated to a higher level in the lung tissues of aged BALB/c mice.

3.2. Multiple inoculation of the mouse-adapted virus caused lethal infection in aged BALB/c mice

GZ08-18 was isolated via plaque purification from the BALF of the 50th passage. In comparison to GZ08-0, GZ08-18 appears to share a similar replication pattern but with an apparently higher peak concentration both in vitro (Supplementary Fig. S2) and in vivo (Supplementary Fig. S3). To compare the pathogenicity in vivo, the aged BALB/c mice with inoculated with 10^{10} $TCID_{50}$ of GZ08-0 or GZ08-18 for 5 times over 3 days as illustrated in Fig. 2A. During the 5-time intra-tracheal inoculation, both GZ08-0-infected and GZ08-18-infected mice underwent comparable body weight loss. However, from day 3 after the last inoculation, GZ08-18-infected mice lost weight more significantly than GZ08-0-infected mice (Fig. 2B), with more prominent disease signs such as ruffled fur, labored breathing, and motionless. On day 6 post infection, 7 out of 11 GZ08-18 mice succumbed to the infection and the remaining 4 mice died on day 7 post infection. On the other hand, all GZ08-0 mice recovered from the 5-time intra-tracheal inoculation and survived the infection (Fig. 2C, $p < 0.005$). Overall, our data demonstrated that multiple intra-tracheal inoculation of the adapted virus GZ08-18, but not the parental virus, resulted in prominent disease and a lethal infection in aged BALB/c mice.

3.3. The mouse-adapted virus replicated more robustly in mouse lung with more significant pathology than the parental virus

To further characterize the infection of GZ08-0 and GZ08-18 in mice, we detected viral titers in BALF and examined the lung pathology of the infected mice. As shown in Fig. 3A, the viral titers in BALF of the GZ08-18-infected mice were significantly higher than those in the GZ08-0-infected mice at day 3 and day 4 post infection. The viral loads detected by RT-qPCR assay showed the same pattern, viral loads were significantly higher in GZ08-18 mice than in GZ08-0 mice at day 3 post infection although the difference was not statistically significant at day 4 post infection (Fig. 3A, right panel). We next examined the viral F protein positive cells in mouse lung tissues at day 3 post infection with immunofluorescence staining. Consistent to our viral titer results, apparently more virus-positive cells were observed in the GZ08-18-infected mice than in the GZ08-0-infected mice (Fig. 3B). Histological examinations revealed evidence of bronchiolitis and pneumonia in both GZ08-0 mice and GZ08-18 mice. The predominant lesion consisted of mononuclear cell infiltration in perivascular and peribronchiolar tissue and thickened alveolar septa (Fig. 3C). Occasionally an exudate composed of desquamated epithelial cells, macrophages, mononuclear cells, and polymorphonuclear cells was observed in the lumen of some bronchioles. Importantly, the lung lesions in GZ08-0-infected mice ameliorated from day 4 post infection whereas the lung pathology persisted in GZ08-18-infected mice.

The HE slides of GZ08-0- and GZ08-18-infected mice was reviewed in a blinded manner by an experienced pathologist and scored with a semi-quantitative protocol as we previously described (Ye et al., 2017). Our data suggested that there were significant differences in lung pathology between GZ08-0- and GZ08-18-infected mice on day 2, day 3, and day 4 post infection (Supplementary Fig. S4). A previous study reported the presence of viral protein and viral RNA in the brain of intra-nasally infected BALB/c mouse (Espinoza et al., 2013). In this regard, we examined the viral loads in the brain and blood of GZ08-18- and GZ08-0-infected mice. However, no viral RNA was detected, suggesting the absence of extra-pulmonary involvement in our mouse model (data not shown). Taken together, we demonstrated that the GZ08-18 virus replicated more robustly and resulted in more prominent lung pathology in the aged BALB/c mice than the parental virus.

3.4. The infection of the mouse adapted virus induced higher levels of pro-inflammatory cytokines and chemokines than that of the parental virus

To compare the inflammatory response in the GZ08-0-infected and GZ08-18-infected mice, the lung homogenates were collected for the quantification of the levels of proinflammatory cytokines and chemokines. In addition, the BALFs were used for the detection of albumin, which is an indicator of tissue injury. As shown in Fig. 4, the GZ08-18-infected mice produced significantly higher levels of IFN-γ, MIP-1α, and TNF-α than that of the GZ08-0-infected mice at multiple time points while the production of RANTES and IFN-β was comparable in the two groups of mice. Consistent to the more prominent lung pathology in the GZ08-18 mice, albumin was significantly elevated in the GZ08-18-infected mice than in the GZ08-0-infected mice at day 3 and day 4 post infection (Fig. 4). Therefore, the results indicated GZ08-18 infection in the aged BALB/c mice induced higher levels of proinflammatory response and more prominent tissue damage than the infection of the parental virus GZ08-0.

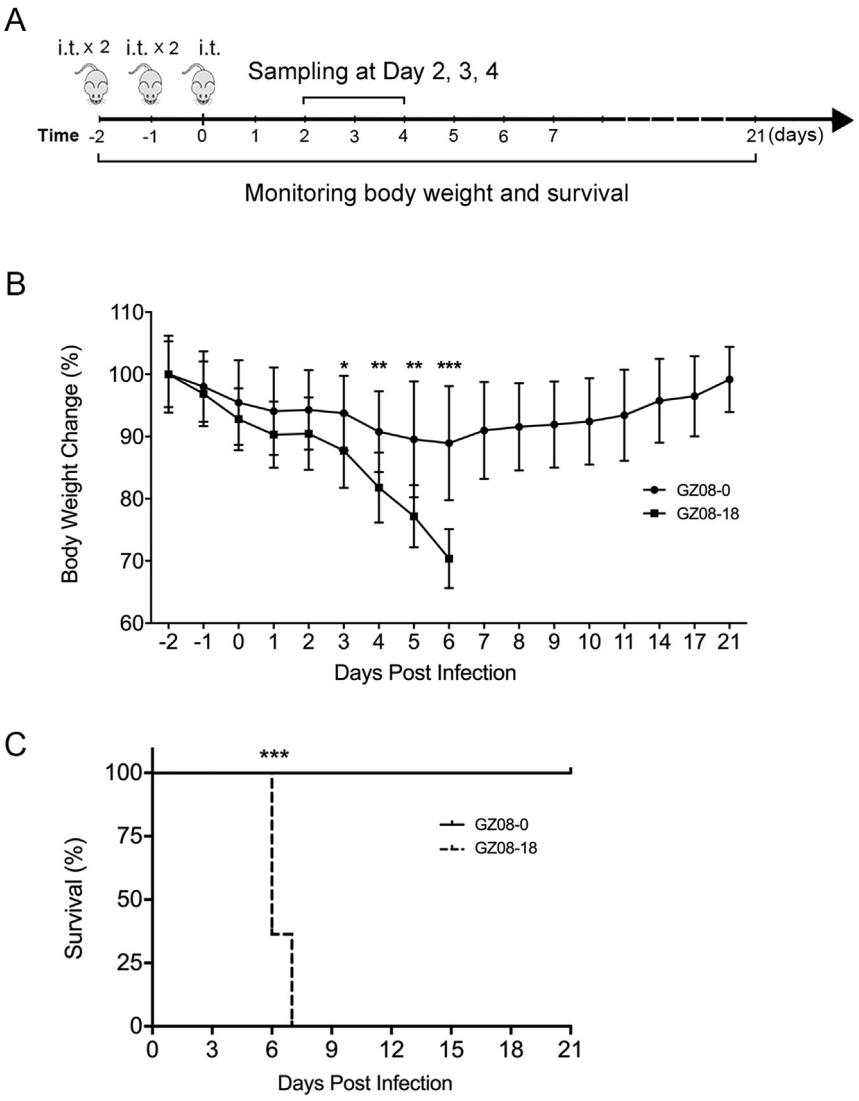

Fig. 2. The mouse-adapted virus GZ08-18 caused significant body weight loss and a lethal infection in aged BALB/c mice. (A) Schematics of the mouse experiment. (B) The body weight change of GZ08-0-inocualted mice (n = 11) and GZ08-18-inoculated mice (n = 11). The data show mean ± SD of live mice at the indicated day. *, **, and *** represent $p < 0.05$, $p < 0.01$, and $p < 0.005$ respectively. (C) The survival rate of GZ08-0 and GZ08-18 inoculated mice was monitored up to day 21 post inoculation. *** represents $p < 0.005$.

3.5. The identification of mutations in the mouse adapted virus GZ08-18

In order to identify mutations in the mouse adapted virus GZ08-18 versus the parental virus GZ08-0, we compared the genomic sequences of GZ08-0 (GenBank accession No: KP218910) and GZ08-18 (GenBank accession No: KP119747). As summarized in Fig. 5, there are a total of 17 mutations between the two virus strains, 12 of them are non-synonymous, 3 (G145A, T6717C, and T12570C) are synonymous, and 2 (A42G and A7484T) are positioned in the non-coding domain. Among the 12 non-synonymous mutations, G gene harbors 5 mutations while the F and L gene each accommodates 2 mutations. The NS1, N, and M gene each carries 1 mutation. Intriguingly, all 17 mutations have not been reported. The bioinformatics program ExPASy was used to analyze the potential functional consequence of these mutations. The result suggested that the Q127R mutation in the G protein created one additional PKC phosphorylation site in GZ08-18, while another non-synonymous mutation in the G protein, K196E, resulted in the disruption of a combined site of amidation and cAMP/cGMP-dependent protein kinase phosphorylation in GZ08-18.

3.6. Pretreatment of cyclophosphamide resulted in a more permissive mouse model

Kong et al. reported that CYP treatment created an immunocompromised condition and rendered BALB/c mice more permissive to HRSV with an exacerbated infection and pathology (Kong et al., 2005). We sought to assess whether CYP treatment can increase the pathogenicity of GZ08-18 and GZ08-0, causing a lethal infection with less rounds of inoculation in aged BALB/c mice since the lethal infection of GZ08-18 can only be achieved after a consecutive 5-time inoculation. Two groups of mice were pretreated with CYP six days prior to the 2-time inoculation of GZ08-0 and GZ08-18 with 12-h interval. Another group of mice was treated with CYP only as a control to evaluate CYP toxicity. As shown in Fig. 6A, all CYP-pretreated GZ08-18-infected mice died by day 7 after infection, while all CYP-pretreated GZ08-0-infected mice recovered from the infection ($p < 0.001$) although they experienced substantial body weight loss (Fig. 6B). Therefore, the CYP pretreatment rendered the aged BALB/c mice more permissive to the mouse-adapted virus, which makes the mouse model more manageable.

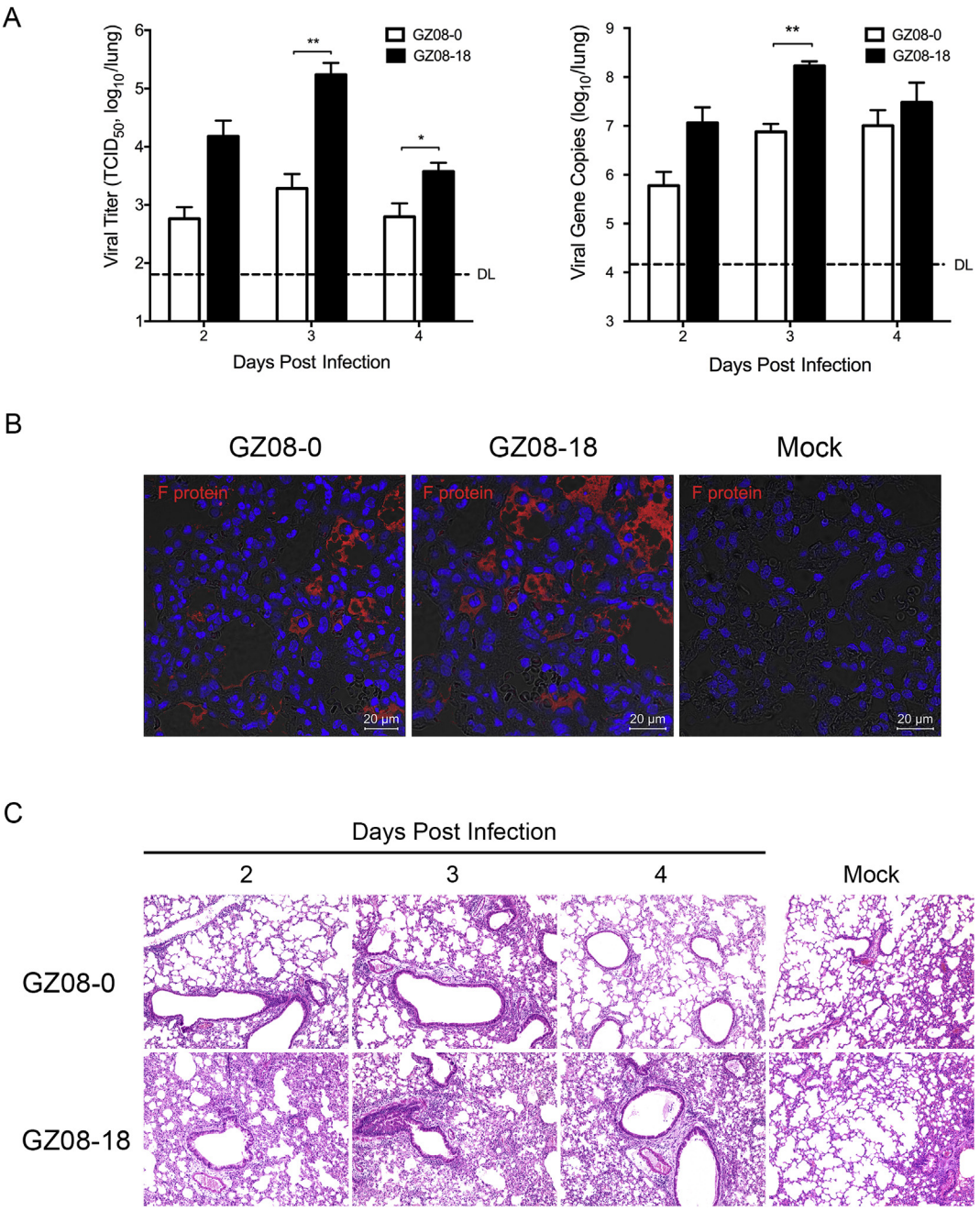

Fig. 3. GZ08-18 replicated more robustly in mouse lung and led to more prominent pathology than the parental virus. (A) BALF samples from GZ08-0 mice and GZ08-18 mice at day 2, day 3, and day 4 post infection were used to assess viral growth by $TCID_{50}$ assay (left) and RT-qPCR assay (right). Data present mean + SD of 3 mice. DL, Detect Limitation. * and ** represent $p < 0.05$ and $p < 0.01$, respectively. (B) The lung tissue slides of GZ08-0 and GZ08-18 mice, together with that of mock-infected mouse were stained with antibody against HRSV F protein (red), counterstained with DAPI (blue) and imaged with confocal microscope. The representative images of GZ08-0 and GZ08-18 mice at day 3 post infection as well as that of a mock-infected mouse are presented. The Mock-infected mouse was intratracheally inoculated with PBS for 5 times. (C) Histopathological examination of lung tissues from GZ08-0- and GZ08-18-infected mice. The images show the representative lung pathology of GZ08-0- and GZ08-18-infected mice at day 2, day 3, and day 4 post infection. H&E staining, magnification 100×.

3.7. The application of the GZ08-18 lethal mouse model in antiviral investigations

We reasoned that the establishment of a lethal HRSV mouse model would be a valuable tool in the future investigations on anti-HRSV regimens. To this end, we demonstrated the capacity of our mouse model in a proof-of-concept study. Mice were inoculated with GZ08-18 for 5 times as illustrated in Fig. 2A. In addition, ribavirin or PBS was injected to the mice via intraperitoneal administration at 3 h post infection after the 2nd, 4th, and 5th virus inoculation. As demonstrated in Fig. 7A, all ribavirin-treated mice survived to day 21 post infection while all PBS-treated mice succumbed to infection by day 7 post virus inoculation. In parallel, the antiviral capacity of ribavirin was also evidenced by the improved body weight change (Fig. 7B) as well as the reduction in virus replication (Fig. 7C). Taken together, our data demonstrated the potential of our lethal mouse model in the future HRSV investigations.

4. Discussion

HRSV is among the most important respiratory pathogens in young

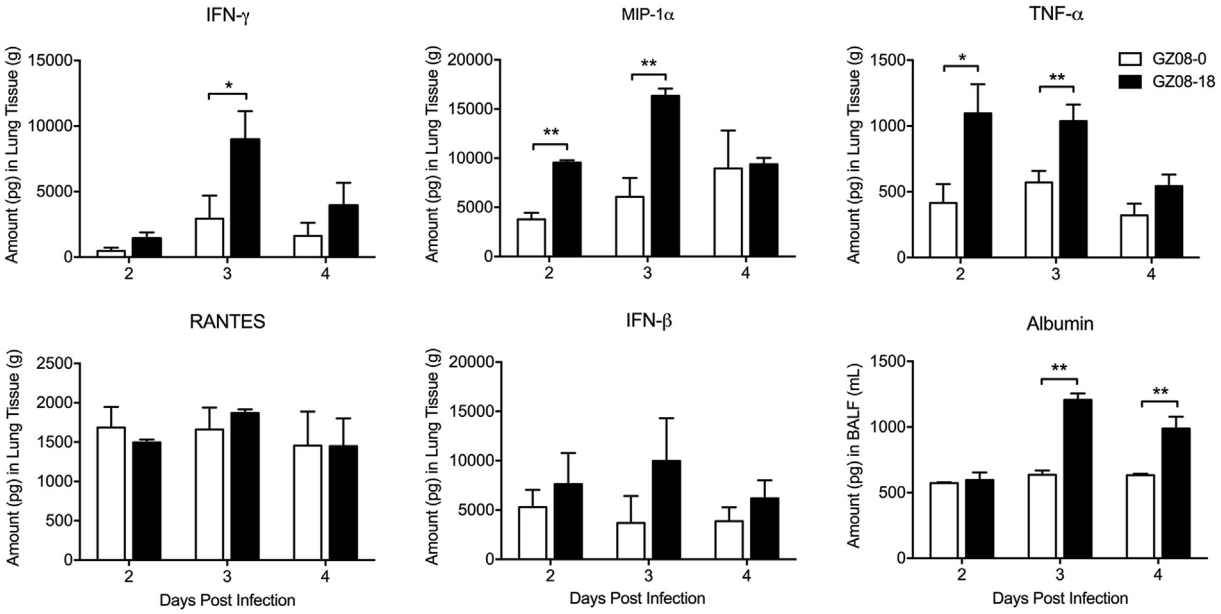

Fig. 4. Inflammatory response in the GZ08-0- and GZ08-18-inoculated mice. The lung homogenates of GZ08-0 and GZ08-18 mice at the indicated days were used for the detection of IFN-γ, MIP-1α, TNF-α, RANTES, and IFN-β by ELISA. The BALF samples of GZ08-0 and GZ08-18 mice were used for measuring albumin by ELISA. Data are presented as mean +SD of 3 mice. * and ** represent $p < 0.05$ and $p < 0.01$, respectively.

children and the elderly worldwide. Unfortunately, despite strenuous efforts, the effective treatment and prevention of HRSV infection remain a significant unmet medical need. The lack of a lethal animal model in the past few decades posed a great hurdle for the development of HRSV vaccines and anti-HRSV drugs. In 2005, Bolger et al. reported the first lethal HRSV model by using a higher titer inoculum (Bolger et al., 2005). However, this model requires substantial efforts for the preparation of virus stock, which may hinder its application in some laboratories. To this end, we seek to establish a more practical lethal mouse model through generating mouse-adapted viruses by passaging the virus in mice. After consecutive passaging of HRSV in aged BALB/c mice, one of the strains, GZ08-18, became more pathogenic than the parental strain. In particular, the GZ08-18-infected mice developed more significant weight lost than the GZ08-0-infected mice with more severe disease manifestations. More importantly, all GZ08-18-infected mice succumbed to infection by day 7 post infection, in contrast to the survival of all GZ08-0-infected mice. Consistent with the survival data, GZ08-18 replicated to significantly higher levels than GZ08-0 as evidenced by detection of viral loads in BALF samples. Accordingly, immunostaining of the lung sections revealed a more extensive and intensive viral fusion protein expression in GZ08-18-infected mice than in GZ08-0-infected mice. Meanwhile, histopathology examination suggested that GZ08-18 caused more prominent lung pathology than GZ08-0. Furthermore, we demonstrated that GZ08-18 induced higher levels of proinflammatory cytokine/chemokine response than that of GZ08-0, indicating the presence of excessive inflammation in the GZ08-18-infected mice. The significantly higher BALF albumin level in GZ08-18-infected mice over GZ08-0-infected mice echoed the more prominent lung pathology in the former mice as revealed by histopathological examination. Overall, we successfully established and characterized a lethal HRSV mouse model. To our knowledge, this is the first HRSV mouse-adapted strain that can cause a lethal infection in BALB/c mice.

In the current mouse model, a series of 5-consecutive intra-tracheal inoculations are required to cause a lethal infection. To potentially decrease the number of inoculations required to reach a lethal infection, we pre-treated the aged BALB/c mice with cyclophosphamide (CYP) to create an immunocompromised status as reported previously (Kong et al., 2005). Consistent to the previous report, CYP pretreatment was unable to result in a lethal infection in the mice inoculated with the parental virus GZ08-0. However, the CYP-pretreated mice succumbed to infection after 2-consecutive intra-tracheal inoculations of GZ08-18. In this regard, these CYP-pretreated mice will be less laborious for evaluating the effect of anti-HRSV drugs. However, cautions must be taken for assessing the efficacy of HRSV vaccine and for elucidating the pathogenesis of HRSV in vivo.

Sequence analysis reveals a total of 17 mutations between GZ08-0 and GZ08-18. Twelve out of the 17 mutations are non-synonymous, which might be related to the elevated pathogenicity of GZ08-18 over its parental strain. The mutation sites are mainly distributed in viral membrane proteins such as G and F gene, as well as N and L gene encoding viral polymerase. Based on the bioinformatics analysis, the Q127R mutation in G protein generated one additional PKC

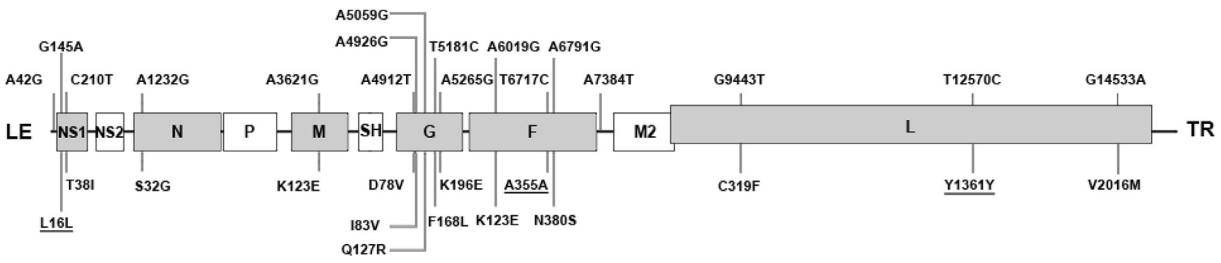

Fig. 5. Distribution of the mutations in the mouse adapted virus GZ08-18 relative to the parental virus GZ08-0. The 17 nucleotide mutations (upside) and 12 non-synonymous amino acid mutations (downside) and 3 synonymous (underlined) ones were denoted in the viral genome. The grey and box boxes represent the coding regions of viral genes with or without mutation(s) respectively, while lines in between refer to the introns. LE, leader; TR, trailer.

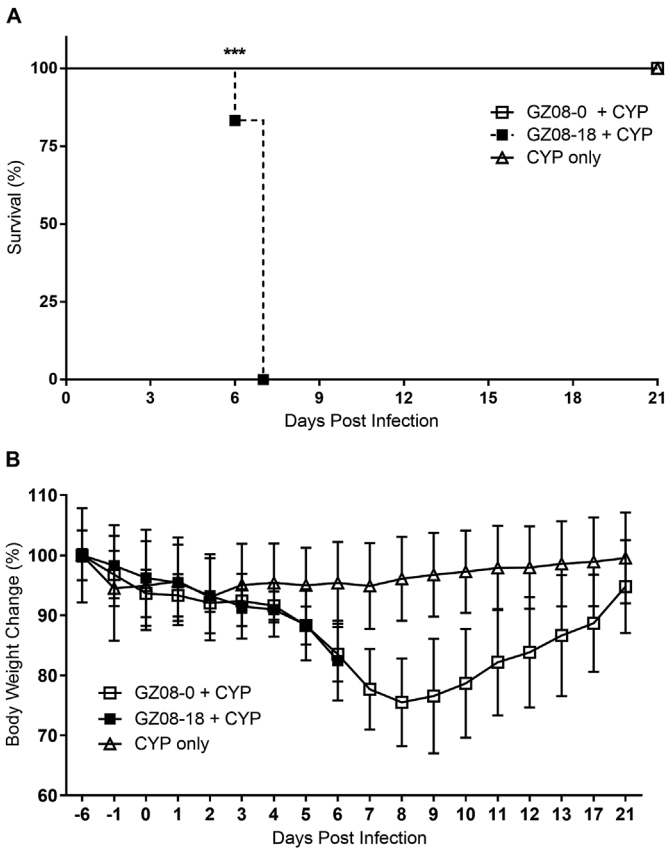

Fig. 6. Pretreatment of cyclophosphamide rendered the GZ08-18 inoculated mice more susceptible to a lethal infection. Two groups of 6 aged BALB/c mice were intraperitoneally injected with 150 mg/kg CYP 6 days prior to 2-time intratracheal inoculation (12 h-interval) of GZ08-0 and GZ08-18. Another group of 6 aged BALB/c mice was intraperitoneally injected with 150 mg/kg CYP as control. (A) The survival rate of GZ08-0-infected CYP pretreated mice (n = 6), GZ08-18-infected CYP pretreated mice (n = 6), and CYP pretreated mice (n = 6) were monitored up to day 21 post infection. *** represents $p < 0.005$. (B) The body weight changes of the above 3 groups of mice were monitored up to day 21 post infection.

phosphorylation site in GZ08-18. Interestingly, San-Juan-Vergara et al. demonstrated that HRSV induced phosphorylation of PKC-α and its cytoplasm-to-membrane translocation, which are required for the virus fusion to the cell membrane and viral entry (Homero San-Juan-Vergara et al., 2005). Therefore, the additive PKC phosphorylation site may enhance the replication capacity and pathogenicity of GZ08-18 over its parent strain. However, the interpretation of bioinformatic analysis, such as the generation of an additional PKC phosphorylation site and disruption of functional domains due to the mutations in G protein, will require further wet lab studies.

Importantly, our lethal HRSV model provided an opportunity to study the pathogenic mechanisms of severe HRSV infections in vivo. In addition, it could also serve as a platform in the investigation of anti-HRSV therapeutic regimens against lethal infections. As exemplified with ribavirin treatment, our model allowed the evaluation of a candidate drug with the survival perimeter, which was not achievable with the previous semi-permissive mouse models.

In conclusion, we successfully established a lethal HRSV mouse model, which was further characterized with virological, immunological, and pathological examinations. We have further demonstrated its potential applications, which will allow future research to evaluate vaccines and candidate drugs against HRSV in BALB/c mice.

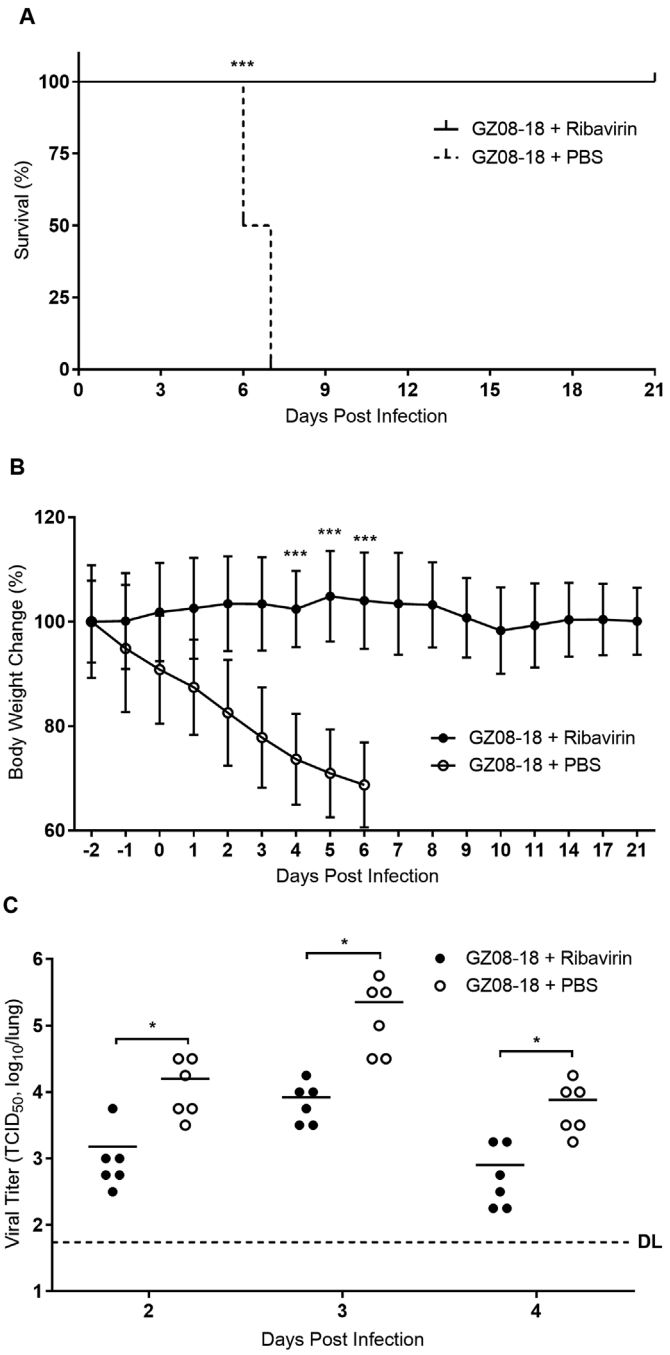

Fig. 7. Ribavirin treatment improved survival rate of GZ08-18-infected mice. Mice were inoculated with GZ08-18 as illustrated in Fig. 2A, and were intraperitoneally injected with Ribavirin (100 mg/kg) or PBS at 3 h after the 2nd, 4th and 5th intra-tracheal virus inoculation. (A) The survival rate of ribavirin-treated GZ08-18-infected mice (n = 10) and PBS-treated GZ08-18-infected mice (n = 8) was monitored up to day 21 post infection. *** represents $p < 0.005$. (B) The body weights of the above two groups of mice were monitored simultaneously. The data showed mean ± SD of the live mice at the indicated day. *** represents $p < 0.005$. (C) BALF samples from ribavirin-treated GZ08-18-infected mice (n = 18) and PBS-treated GZ08-18-infected mice (n = 18) at day 2, day 3, and day 4 post infection were used to assess viral growth by $TCID_{50}$ assays. DL, Detect Limitation. * represents $p < 0.05$.

Conflicts of interest

The authors have declared that no conflict of interest exists.

Author contributions

B.Z., K.Z. J.Z., and H.C. conceived the study. K.Z., C.L., Y-S.L., S.Y., D.W., B.H-Y.W., X.Z., M.C.C., Z-W.Y., Z.S, H.Z., X.Z., M.H., D.Y., H.S., and Y.W. performed the experiments. K.Z., C.L., Y-S.L., L.W., H.C., and J.Z. analyzed and interpreted the data. J.H., M.E.B., and K.J.H performed sequencing of virus genome. J.Z., H.C., K.Z., B.Z., and J-D.H. wrote and revised the manuscript.

Funding

This work was partly supported by National Natural Science Foundation of China (81860752); Research Fund for the Control of Infectious Diseases (RFCID, 10091222) and Health and Medical Research Fund (HMRF, 14131392) of Food and Health Bureau, Hong Kong Special Administrative Region; Collaborative Research Fund (C7011-15R) of the Research Grants Council, Hong Kong Special Administrative Region; Joint Foundation of Collaboration Project between Scientific and Technological Department of Guizhou Province and Colleges/Universities of Guizhou Province (LH[2015]7349); and the Training Project of Young Scientific Talent of Education Department of Guizhou Province (KY[2016]147).

Appendix A. Supplementary data

Supplementary data to this article can be found online at https://doi.org/10.1016/j.antiviral.2018.11.015.

References

Bolger, G., Lapeyre, N., Dansereau, N., Lagacé, L., Berry, G., Klosowski, K., Mewhort, T., Liuzzi, M., 2005. Primary infection of mice with high titer inoculum respiratory syncytial virus: characterization and response to antiviral therapy. Can. J. Physiol. Pharmacol. 83, 198–213.

Chu, H., Chan, C.M., Zhang, X., Wang, Y., Yuan, S., Zhou, J., Au-Yueng, R.K., Sze, K.H., Yang, D., Shuai, H., Hou, Y., Li, C., Zhao, X., Poon, V.K., Leung, S.P., Yeung, M.L., Yan, J., Lu, G., Jin, D.Y., Gao, G.F., Chan, J.F., Yuen, K.Y., 2018. Middle East respiratory syndrome coronavirus and bat coronavirus HKU9 both can utilize GRP78 for attachment onto host cells. J. Biol. Chem. 293 (30), 11709–11726 Jul 27.

Chu, H., Zhou, J., Wong, B.H., Li, C., Chan, J.F., Cheng, Z.S., Yang, D., Wang, D., Lee, A.C., Li, C., Yeung, M.L., Cai, J., Chan, I.H., Ho, W.K., To, K.K., Zheng, B.J., Yao, Y., Qin, C., Yuen, K.Y., 2016. Middle East respiratory syndrome coronavirus efficiently infects human primary T lymphocytes and activates both the extrinsic and intrinsic apoptosis pathways. J. Infect. Dis. 213 (6), 904–914 Mar 15.

Daubeuf, F., Frossard, N., 2012. Performing bronchoalveolar lavage in the mouse. Curr. Protoc. Mouse Biol. 2, 167–175.

Do, L.A.H., Doorn, H.R.V., Bryant, J.E., Nghiem, M.N., Van, V.C.N., Cong, K.V., Nguyen, M.D., Tran, T.H., Farrar, J., Jong, M.D.D., 2012. A sensitive real-time PCR for detection and subgrouping of human respiratory syncytial virus. J. Virol. Methods 179, 250–255.

Dupage, M., Dooley, A.L., Jacks, T., 2009. Conditional mouse lung cancer models using adenoviral or lentiviral delivery of Cre recombinase. Nat. Protoc. 4, 1064–1072.

Espinoza, J.A., Bohmwald, K., Céspedes, P.F., Gómez, R.S., Riquelme, S.A., Cortés, C.M., Valenzuela, J.A., Sandoval, R.A., Pancetti, F.C., Bueno, S.M., 2013. Impaired learning resulting from respiratory syncytial virus infection. Proc. Natl. Acad. Sci. Unit. States Am. 110, 9112–9117.

Falsey, A.R., Hennessey, P.A., Formica, M.A., Cox, C., Walsh, E.E., 2005. Respiratory syncytial virus infection in elderly and high-risk adults. N. Engl. J. Med. 352, 1749–1759.

Graham, B.S., 2011. Biological challenges and technological opportunities for respiratory syncytial virus vaccine development. Immunol. Rev. 239, 149–166.

Graham, B.S., Perkins, M.D., Wright, P.F., Karzon, D.T., 1988. Primary respiratory syncytial virus infection in mice. J. Med. Virol. 26, 153–162.

Homero San-Juan-Vergara, M.E.P., Lockey, Richard F., Mohapatra, Shyam S., 2005. Protein kinase C-α activity is required for respiratory syncytial virus fusion to human bronchial epithelial cells. J. Virol. 78, 13717–13726.

Jordan, R., Shao, M., Mackman, R.L., Perron, M., Cihlar, T., Lewis, S.A., Eisenberg, E.J., Carey, A., Strickley, R.G., Chien, J.W., Anderson, M.L., McEligot, H.A., Behrens, N.E., Gershwin, L.J., 2015. Antiviral efficacy of a respiratory syncytial virus (RSV) fusion inhibitor in a bovine model of RSV infection. Antimicrob. Agents Chemother. 59, 4889–4900.

Kong, X., Hellermann, G.R., Patton, G., Kumar, M., Behera, A., Randall, T.S., Zhang, J., Lockey, R.F., Mohapatra, S.S., 2005. An immunocompromised BALB/c mouse model for respiratory syncytial virus infection. Virol. J. 2, 3.

McKimm-Breschkin, J.L., 2004. A simplified plaque assay for respiratory syncytial virus—direct visualization of plaques without immunostaining. J. Virol Methods 120, 113–117.

Nair, H., Nokes, D.J., Gessner, B.D., Dherani, M., Madhi, S.A., Singleton, R.J., O'Brien, K.L., Roca, A., Wright, P.F., Bruce, N., Chandran, A., Theodoratou, E., Sutanto, A., Sedyaningsih, E.R., Ngama, M., Munywoki, P.K., Kartasasmita, C., Simoes, E.A., Rudan, I., Weber, M.W., Campbell, H., 2010. Global burden of acute lower respiratory infections due to respiratory syncytial virus in young children: a systematic review and meta-analysis. Lancet 375, 1545–1555.

Shaw, C.A., Galarneau, J.-R., Bowenkamp, K.E., Swanson, K.A., Palmer, G.A., Palladino, G., Markovits, J.E., Valiante, N.M., Dormitzer, P.R., Otten, G.R., 2013. The role of non-viral antigens in the cotton rat model of respiratory syncytial virus vaccine-enhanced disease. Vaccine 31, 306–312.

Sow, F.B., Gallup, J.M., Olivier, A., Krishnan, S., Patera, A.C., Suzich, J., Ackermann, M.R., 2011. Respiratory syncytial virus is associated with an inflammatory response in lungs and architectural remodeling of lung-draining lymph nodes of newborn lambs. Am. J. Physiol. Lung Cell Mol. Physiol. 300, L12–L24.

Sun, Z., Lu, S., Yang, Z., Li, J., Zhang, M.Y., 2017. Construction of a recombinant full-length membrane associated IgG library. Virus Res. 238, 156–163.

Tang, R.S., MacPhail, M., Schickli, J.H., Kaur, J., Robinson, C.L., Lawlor, H.A., Guzzetta, J.M., Spaete, R.R., Haller, A.A., 2004. Parainfluenza virus type 3 expressing the native or soluble fusion (F) Protein of Respiratory Syncytial Virus (RSV) confers protection from RSV infection in African green monkeys. J. Virol. 78, 11198–11207.

Taylor, G., Stott, E., Hughes, M., Collins, A., 1984. Respiratory syncytial virus infection in mice. Infect. Immun. 43, 649–655.

Teng, M.N., Whitehead, S.S., Bermingham, A., St Claire, M., Elkins, W.R., Murphy, B.R., Collins, P.L., 2000. Recombinant respiratory syncytial virus that does not express the NS1 or M2-2 protein is highly attenuated and immunogenic in chimpanzees. J. Virol. 74, 9317–9321.

Thompson, W.W., Shay, D.K., Weintraub, E., Brammer, L., Cox, N., Anderson, L.J., Fukuda, K., 2003. Mortality associated with influenza and respiratory syncytial virus in the United States. J. Am. Med. Assoc. 289, 179–186.

Ye, Z.W., Yuan, S., Poon, K.M., Wen, L., Yang, D., Sun, Z., Li, C., Hu, M., Shuai, H., Zhou, J., Zhang, M.Y., Zheng, B.J., Chu, H., Yuan, K.Y., 2017. Antibody-dependent cell-mediated cytotoxicity epitopes on the hemagglutinin head region of pandemic h1n1 influenza virus play detrimental roles in H1N1-infected mice. Front. Immunol. 8 (1), 317. https://doi.org/10.3389/fimmu.2017.00317.

Zhang, K., He, J., Li, C., Bose, M.E., Henrickson, K.J., Zhou, J., Zheng, B.J., 2015. Complete genome sequences of one human respiratory syncytial antigenic group a virus from China and its four mouse-adapted isolates. Genome Announc. 3.

Zhou, J., Chu, H., Li, C., Wong, B.H., Cheng, Z.S., Poon, V.K., Sun, T., Lau, C.C., Wong, K.K., Chan, J.Y., Chan, J.F., To, K.K., Chan, K.H., Zheng, B.J., Yuen, K.Y., 2014. Active replication of Middle East respiratory syndrome coronavirus and aberrant induction of inflammatory cytokines and chemokines in human macrophages: implications for pathogenesis. J. Infect. Dis. 209, 1331–1342.